Heterogeneous Catalysis Mediated Cofactor NADH Regeneration for Enzymatic Reduction

Xiaodong Wang[1] and Humphrey H. P. Yiu*

Chemical Engineering, School of Engineering & Physical Sciences, Heriot-Watt University, Edinburgh EH14 4AS, Scotland, United Kingdom

*corresponding author e-mail: H.H.Yiu@hw.ac.uk

[1]present address: School of Engineering, College of Physical Sciences, University of Aberdeen, Aberdeen AB24 3UE, Scotland, United Kingdom

Abstract

Enzymatic reduction using oxidoreductases is important in commercial chemical production. This enzymatic action requires a cofactor (e.g. NADH) as hydrogen source that is consumed during reaction and must be regenerated. We present, for the first time, an *in situ* NADH regeneration ($NAD^+ \rightarrow$ NADH) using a heterogeneous catalyst (Pt/Al_2O_3) and H_2 coupled with an enzymatic reduction. This regeneration system can be operated at ambient pressure where NADH yield and turnover frequency (*TOF*) increased with temperature (20-37 °C) and pH (4.0-9.9) delivering full selectivity to enzymatically active NADH. Cofactor regeneration by heterogeneous catalysis represents a cleaner (H^+ as sole by-product) alternative to current enzymatic and homogeneous (electro- and photo-) catalytic methods with the added benefit of facile catalyst separation. The viability of coupling cofactor regeneration with enzymatic (alcohol dehydrogenase, ADH) reaction is established in aldehyde reduction (propanal to propanol) where 100% alcohol yield was achieved. The potential of this hybrid inorganic-enzymatic system is further demonstrated in the continuous (fed-batch) conversion of propanal with catalyst (activity/selectivity) stability for up to 100 h.

Keywords: cofactor NADH regeneration, Pt/Al_2O_3, hydrogenation, dehydrogenase, carbonyl reduction

1. Introduction

Enzymatic technologies are extensively employed in the manufacture of chemicals and pharmaceuticals.[1] More than a quarter of commercial enzymes are oxidoreductases[2] that operate in tandem with a cofactor, typically nicotinamide adenine dinucleotide (NADH) or its phosphorylated form (NADPH). In the enzymatic reaction cycle, NADH serves as hydrogen donor with a resultant oxidation to NAD^+, as illustrated by pathway **(a)** in **Figure 1**. Given the high cost of NADH (bulk price per mole: US$3,000),[3] a stoichiometric supply for commercial enzymatic transformations is not economically feasible and regeneration (NAD^+ → NADH, pathway **(b)** in **Figure 1**) is required. Coupled-enzyme methodologies employ two separate enzymes for substrate → product reduction and cofactor regeneration.[4] Commercial processes use glucose or formate dehydrogenases (GDH or FDH) as regeneration enzymes while phosphite and alcohol dehydrogenases have been applied at laboratory scale.[4] The generation of significant quantities of water-soluble by-products (196 g gluconic acid per mol NADH regenerated by GDH and 44 g CO_2 per mol NADH regenerated by FDH),[4a] costly downstream separation and enzyme deactivation are decided drawbacks. Moreover, there is a requirement for base or acid addition to maintain the optimal pH (*ca.* 7.0)[5] for enzymatic action.[6] Non-enzymatic NADH regenerations have also been reported employing inorganic reductants (*e.g.* $Na_2S_2O_4$ and $NaBH_4$),[7] homogeneous catalysis (*e.g.* Ru, Rh and Ir complexes),[8] photocatalysis (*e.g.* copolymers and carbon nitride)[9] and electrocatalysis (including both direct regeneration on the electrode[10] and indirect regeneration using organometallic complexes as hydrogen transfer agents[11]). Some of these methodologies suffer from low selectivity with irreversible formation of inactive NAD_2 (pathway **(c)** in **Figure 1**) and/or 1,6-NADH (pathway **(d)** in **Figure 1**).[8b,9b,c,10] There are also issues of sustainability associated with the requirement for electron mediators,

photosensitizers, sacrificial organic electron donors and toxic organometallic complexes which necessitate energy-intensive separation stages.[4a,7,12] Therefore, these non-enzymatic approaches have only been studied at a laboratory scale and not used in industries.

In this work we demonstrate an alternative, novel strategy for NADH regeneration using a heterogeneous (supported metal) catalyst that generates H^+ *as sole by-product*. As supported Pt has shown activity in the hydrogenation of compounds with similar ring structure to NADH (*e.g.* pyridines),[13] we have investigated a commercial Pt/Al_2O_3 catalyst with H_2 as reductant (see pathway **(b)** in **Figure 1**). This is the first application of supported metal catalyst for cofactor regeneration. We should however flag reports in the literature dealing with (immobilized) enzymatic regeneration using H_2[12a, 14] and photocatalytic[15] and electrocatalytic[16] regeneration using Pt nanoparticles as photosensitizer and proton carrier, respectively. In this study we couple NADH regeneration by Pt/Al_2O_3 with continuous conversion of propanal to propanol over alcohol dehydrogenase as a model enzymatic redox transformation. We probe the effect of temperature, pH and H_2 pressure in the regeneration step. Our proposed hybrid synthetic-biocatalytic system can serve as a new route for the production of chemicals by NADH dependent enzymes.

2. Experimental

2.1. Materials

β-Nicotinamide adenine dinucleotide hydrate (NAD^+, ≥96.5%), β-nicotinamide adenine dinucleotide reduced disodium salt hydrate (NADH, ≥94%), KH_2PO_4 (≥99%), K_2HPO_4 (≥98%), DL-6,8-thioctic acid amide (DL-lipoamide, ≥99%), ethylenediaminetetraacetic acid (EDTA) tetrasodium salt hydrate (≥95%), albumin from bovine serum (≥96%), diaphorase from *Clostridium kluyveri* (100-UN), alcohol dehydrogenase from *Saccharomyces cerevisiae*, deuterium oxide (D_2O, ≥99.9%) and Pt/Al_2O_3 (1% w/w) were obtained from Sigma-Aldrich.

Propanal (≥99%), propanol (≥99%), and ethanol (≥99.8%) were supplied by Fisher Scientific. All the chemicals were used as received without further purification. The gases (H_2, N_2, and He, BOC) were ultra-high purity (>99.99%).

2.2. Catalyst characterization

Nitrogen adsorption-desorption isotherms (at –196 °C) were obtained using the commercial automated Micromeritics Gemini VII 2390p system. Specific surface area was obtained from the adsorption isotherms using the standard BET method. Total pore volume (P/P_0 = 0.95) and mean pore size was determined by BJH analysis of the desorption isotherms; samples were outgassed at 150 °C under N_2 for 1 h prior to measurement. Temperature programmed treatment and H_2 chemisorption were recorded on the commercial CHEMBET 3000 (Quantachrome Instrument) equipped with a thermal conductivity detector (TCD) and TPR Win^{TM} software for data acquisition/manipulation. The Pt/Al_2O_3 catalyst was loaded into a U-shaped quartz cell (3.76 mm *i.d.*), heated to reaction temperature (37 °C) under N_2 and subjected to H_2 (BOC, 99.99%) pulse (10-50 μl) titration. The H_2 pulses were continued until the signal area was constant, indicating surface saturation. The as received sample was subjected to thermal treatment in 17 cm^3 min^{-1} (Brooks mass flow controlled) 5% v/v H_2/N_2 at 5 °C min^{-1} to 350 °C for 1 h. The sample was swept with 65 cm^3 min^{-1} N_2 for 1.5 h, cooled to 37 °C and subjected to H_2 titration as above. Platinum particle morphology (size and shape) was determined by scanning transmission electron microscopy (STEM, JEOL 2200FS field emission gun-equipped TEM unit), employing Gatan DigitalMicrograph 1.82 for data acquisition/manipulation. By using an annular bright/dark field detector with a minimum collection semi-angle of ~100 mrad, the recorded images showed an intensity approximately proportional to $tZ^{1.7–2}$ (sample thickness t, average atomic number Z), facilitating clear contrast between the heavy and lighter element components. Samples for

analysis were prepared by dispersion in acetone and deposited on a holey carbon/Cu grid (300 Mesh). The number weighted mean metal particle size (d) was obtained from

$$d = \frac{\sum_i n_i d_i}{\sum_i n_i} \quad \textbf{(1)}$$

where n_i is the number of particles of diameter d_i with Σn_i =440.

2.3. NADH analysis

NADH concentration was monitored by UV-Vis spectrophotometry (Shimadzu, UVmini-1240) at λ = 340 nm.[15,17] In order to discount any contribution to the UV signal from inactive by-products (NAD_2 and 1,6-NADH) an independent validation of NADH yield was required to establish exclusive generation of active NADH. An enzymatic assay using lipoamide dehydrogenase based on Sigma Quality Control Test Procedure EC 1.8.1.4 has been established as an effective means of NADH determination[18] and was employed in this work to identify and quantify NADH concentration. Lipoamide dehydrogenase is specific to NADH and does not act on NAD_2 or 1,6-NADH and only the active NADH is consumed according to

$$\text{NADH + DL-lipodamide} \rightarrow \text{NAD}^+ + \text{DL-6,8-dihydrothioctic acid amide} \quad \textbf{(2)}$$

with UV absorbance directly proportional to NADH concentration. The assay was carried out at T = 25 °C and pH = 7.0. The following reagents were prepared: **(A)** 0.1 M phosphate buffer solution (pH = 7.0 at 25 °C) from KH_2PO_4 and K_2HPO_4 in deionized water; **(B)** 28 mM DL-6,8-thioctic acid amide solution (DL-Thio, substrate for assay) by dissolving 57.4 mg DL-6,8-thioctic acid amide in 6 cm^3 ethanol (non-denatured) and dilution with 4 cm^3 phosphate buffer (reagent A); **(C)** 300 mM ethylenediaminetetraacetic acid (EDTA) solution with 2.0% (w/v) albumin (pH = 7.0 at 25°C) by addition of EDTA and albumin to 10 cm^3

deionized water and pH adjustment with 5 M HCl; **(D)** product mixture from reaction; **(E)** 1.0 unit cm^{-3} lipoamide dehydrogenase (LDH) solution in cold phosphate buffer (reagent A) to avoid denaturation; **(F)** positive control solution with NADH and NAD^+ in the phosphate buffer at the same concentration as the product mixture (D). The sample solutions are summarized in **Table 1**. Additional product analysis by ^1H NMR was conducted on a Bruker AVIII (300 MHz) spectrometer at room temperature and reported in ppm with respect to D_2O as internal standard.

2.4. NADH regeneration

$NAD^+ \rightarrow$ NADH regeneration was carried out in a Parr®5500 compact reactor (with a Parr®4848 reactor controller) at 20-60 °C, pH = 4.0-9.9 and over the (H_2) pressure range 1-9 atm. In a typical experiment, Pt/Al_2O_3 (25 mg) and 50 cm^3 0.1 M phosphate buffered solution containing NAD^+ (1.5 mM) were loaded in the reactor. The system was flushed (three times) with N_2 and the temperature (20-60 °C) allowed to stabilize. Hydrogen gas was then introduced, the system pressurized and stirring (at 900 rpm) engaged (time $t = 0$ for reaction). A non-invasive liquid sampling system via syringe/in-line filters allowed a controlled removal of aliquots from the reactor. NADH yields were calculated from

$$\text{NADH yield (\%)} = \frac{[\text{NADH}]}{[\text{NAD}^+]_0} \times 100 \qquad \textbf{(3)}$$

Catalytic regeneration is also quantified in terms of initial rates obtained from a linear regression of temporal NADH concentration profiles[19] with turnover frequency (*TOF,* rate per active site) calculated using Pt dispersion obtained from STEM analysis.

2.5. Propanal conversion with in situ cofactor regeneration

In the combined NADH regeneration and enzymatic conversion of propanal, experiments were carried out at atmospheric pressure using a commercial glass reactor (Ken

Kimble Reactors Ltd.) coupled with a coolant-condenser system operated at –20 °C. At the start of each reaction alcohol dehydrogenase (1 mg, from *Saccharomyces cerevisiae*), NADH (250 mg), Pt/Al_2O_3 (25 mg) and phosphate buffered solution (50 ml, 0.1 M, pH = 8.8) were loaded into the reactor with a N_2 sparge at 30 cm^3 min^{-1}. The temperature was allowed to stabilize (at 20 °C), the solution sparged with H_2 (30 cm^3 min^{-1}) and agitated at 900 rpm with addition of 36 μL (0.5 mmol) propanal; at time t = 0, propanal concentration ($[propanal]_0$) = 10 mM. For the fed-batch process of enzymatic reduction of propanal with *in situ* cofactor regeneration (T = 20°C, P = 1 atm, pH = 8.8 and initial NADH = 25 μmol) a syringe pump (KD Scientific) supplied a continuous propanal feed (2 mM in phosphate buffer) at 2.5 cm^3 h^{-1}. The composition of the product mixture was analyzed by gas chromatography (Perkin-Elmer Clarus 580 GC) employing a programmed split injector, flame ionization detector (FID) and DB-WAX (30 m × 0.25 mm i.d. 0.25 μm film thickness) capillary column (J&W Scientific). Propanol yield was calculated from

$$\text{Propanol yield (\%)} = \frac{[\text{Propanol}]}{[\text{Propanal}]_0} \times 100 \qquad \textbf{(4)}$$

Enzymatic activity is also quantified in terms of initial conversion obtained from the time on-stream measurements.[19] Replicated reactions delivered raw data reproducibility to within ±7 %.

3. Results and discussion

The critical physicochemical characteristics of the as received Pt/Al_2O_3 are given in **Table 2**. The structural measurements (specific surface area = 162 m^2 g^{-1}, pore volume = 0.40 cm^3 g^{-1} and mean pore size = 7.8 nm) match those reported in the literature.[20] As we use H_2 as reductant in cofactor regeneration, a critical catalyst property in this application is H_2 chemisorption capacity. The measured H_2 uptake (4.1 μmol g^{-1}) is comparable to that reported for hydrogenation active alumina supported catalysts (*e.g.* 4 μmol g^{-1} for Ni/Al_2O_3[21]).

The representative STEM image given in **Figure 2** shows pseudo-spherical Pt particles at the nanoscale (<1-7 nm) with a mean diameter (2.2 nm) that is known to deliver high H_2 uptake.[22]

3.1. Cofactor regeneration by heterogeneous catalysis

We first assessed the viability of the proposed catalytic cofactor regeneration route by carrying out batch reduction of NAD^+ over Pt/Al_2O_3 in H_2. The results are presented in **Figure 3(a)** where the level of reproducibility can be assessed from the error bars generated for five replicated runs. The experimental measurements show an increase in the yield of NADH with time. The results from validation using the EC 1.8.1.4 enzymatic assay (see section *2.3.*) are presented in **Figure 3(b)** and demonstrate that the product generated from catalytic treatment exhibited the same assay response to the NADH/NAD^+ mixture prepared from commercial samples on the basis of UV analysis. The convergence of both sets of results confirms that the catalytic reduction of NAD^+ is fully selective to NADH. ^{1}H NMR spectroscopy analysis was used to further demonstrate selective cofactor regeneration. The ^{1}H NMR spectra for NAD^+ (**Figure 4(a)**) and NADH (**Figure 4(b)**) present characteristic signals at 9.33 and 6.96 ppm, respectively.[23] The ^{1}H NMR spectrum of the product mixture after 6 h (**Figure 4(c)**) presents the same signals where the NADH yield determined coincided with UV measurement (see **Figure 3(a)**). This exclusivity in NADH regeneration is an important finding given the number of published studies where the formation of undesired by-products (*e.g.* NAD_2 and 1,6-NADH) has been reported.[8b,9b,c,10] Dissociative H_2 chemisorption on supported Pt provides surface reactive hydrogen that acts to reduce NAD^+ to NADH (**Figure 1** pathway **(b)**) with the formation of H^+ as by-product, which is buffered in the reaction mixture. This is in contrast to conventional enzymatic regenerations where the formation of

water-soluble by-products requires labor-intensive downstream separation and purification steps.

Temperature, pH and pressure are critical reaction parameters that impact on enzymatic performance.[3] The influence of each variable in our catalytic regeneration process is shown in **Figure 5**. NADH yield **(i)** and specific activity in terms of turnover frequency (*TOF*) **(ii)** were temperature dependent (**Figure 5(a)**). Over a typical temperature range for enzymatic reactions (20 to 37 °C),[24] temporal NADH yield showed an increase with temperature. At a higher reaction temperature (60 °C) a maximum yield was observed after 1.5 h with a decrease thereafter that can be linked to reduction of the nicotinamide ring. A temperature maximum (40 °C) in NAD^+ conversion during enzymatic regeneration using a redox mediator (flavin adenine dinucleotide) has been reported and attributed to deactivation of FDH by the electron mediator.[25] In order to account for the response at 60 °C we monitored catalytic regeneration at extended reaction times (up to 24 h). We should stress that regeneration procedures reported in the literature have been limited to shorter duration, from 2[9b,26] to 12 h[15]. Analysis of the reaction mixture after 6 h by ^{1}H NMR (**Figure 4(d)**) showed no signal due to NAD^+ (δ = 9.33 ppm) consistent with increased activity at higher temperatures (**Figure 5(aii)**) and the appearance of signals at 1-2 ppm. The intensity of these signals increased after 24 h with no detectable NADH (δ = 6.96 ppm) (**Figure 4(e)**). Peaks at 1-2 ppm are characteristic of saturated hydrocarbons[27] and can be attributed to product(s) resulting from hydrogenation of the nicotinamide ring. Our results confirm that NADH regeneration is temperature dependent with undesired ring hydrogenation at 60 °C. Subsequent tests were conducted at $T \leq 37$ °C to avoid non-selective cofactor transformation.

Our regeneration system also showed a pH dependence (**Figure 5(b)**) where an increase in pH from 4.0 to 9.9 resulted in substantial enhancement in NADH yield with an associated

increase in *TOF*. A basic environment serves to neutralize and remove H^+ released in the regeneration step (**Figure 1(b)**) shifting the reaction in favor of NADH formation. A similar pH effect (from 6.0 to 10.0) has been reported for photocatalytic cofactor regeneration.[9b] We should note that Ir complex (homogeneous) catalyzed NADH regeneration at pH = 4–10 with a maximum at pH = 6.5.[17] Rate inhibition was shown at pH > 8. This is in contrast to our system where higher pH favors higher conversion. An increase in H_2 pressure (1-9 atm) served to increase NADH yield and *TOF* (**Figure 5(c)**). This can be ascribed to enhanced H_2 availability in the aqueous medium. The higher *TOF* on raising system pressure from 1 to 5 atm matches the increase in hydrogen solubility (0.0138 *vs.* 0.0875 $cm^3\ g^{-1}$).[28] Further pressure elevation (to 9 atm, H_2 solubility = 0.154 $cm^3\ g^{-1}$) did not result in a proportional increase in rate. An overriding practical consideration for cofactor regeneration when coupled with enzymatic reaction is operation at ambient pressure.[4a] The as received catalyst delivered a *TOF* (4 h^{-1}) under ambient conditions and was increased to 13 h^{-1} (**Figure 5(d)**) following thermal treatment of the catalyst (to 350 °C) in H_2. The treated Pt/Al_2O_3 exhibited equivalent structural characteristics (see **Table 2**) but with a significantly higher level (5-fold) of H_2 chemisorption which can be linked to further reduction of surface Pt to the metallic form with greater H_2 uptake capacity and a consequent increased NADH regeneration rate. In summary, we have established the viability of NADH regeneration using Pt/Al_2O_3 with H_2 as reductant under conditions that are suitable for enzymatic reaction. The regeneration rate (12 μmol $min^{-1}\ mg^{-1}$) over Pt/Al_2O_3 is six times higher than NAD^+-reducing hydrogenase (2 μmol $min^{-1}\ mg^{-1}$)[29] and comparable with values reported for homogeneous organometallic catalysts (13 h^{-1} in this work relative to 10 h^{-1} with formate,[26] 18 h^{-1} using ethanol[30] and 36 h^{-1} using H_2[17]) but those systems exhibit incompatibilities between the organometallics and NADH dependent enzymes that result in enzyme deactivation.[31] Regeneration using immobilized

organometallic catalyst $[Cp^*Rh(bpy)(H_2O)]^{2+}$ has also been reported but showed a maximum *TOF* of 2.5 h^{-1} at 30 °C,[32] five times lower than our system.

3.2. Batch enzymatic propanal reduction with in situ cofactor regeneration

Practical viability of cofactor regeneration requires applicability *in situ* in tandem with a biocatalytic process. Taking this as our goal, we have developed a "one-pot" system that combines NADH regeneration by heterogeneous catalysis with enzymatic (alcohol dehydrogenase) conversion of propanal to propanol as model reaction. The results of the combined cofactor regeneration and propanal transformation are presented in **Table 3** and **Figure 6**. As a blank test (control experiment), propanal conversion (in H_2) over Pt/Al_2O_3 delivered a rate four orders of magnitude lower than that achieved with alcohol dehydrogenase (**Table 3**, rows **1** and **2**). This result demonstrates that propanal transformation is governed by the enzyme and is consistent with the equivalent propanol production rate obtained in the one-pot system with or without Pt/Al_2O_3 (**Table 3**, rows **2** and **3**). The production of propanol is limited by the available NADH concentration and without Pt/Al_2O_3 addition propanol yield reached an upper limit of 70%. Cofactor regeneration by Pt/Al_2O_3 extended alcohol production beyond the initial NADH/propanal stoichiometry to reach full conversion (100% yield, **Figure 6**). The rate of propanol production over the combined Pt/Al_2O_3 and cofactor (0.100 μmol min^{-1}) at the point the two profiles deviate ($t >$ 5 min) matched the rate of NAD^+ reduction by Pt/Al_2O_3 (0.095 μmol min^{-1}). The hydrogenation performance of the coupled system is ultimately controlled by the rate of NADH regeneration. The heterogeneous catalyst (Pt/Al_2O_3) plays an exclusive role in regenerating the NADH cofactor which regulates enzymatic production of the alcohol.

3.3. Continuous enzymatic propanal reduction with in situ cofactor regeneration in a fed-batch setup

In order to realize the full potential of this *in situ* cofactor regeneration strategy we investigated the feasibility of fed-batch propanol production using a fixed starting amount of NADH with continuous propanal supply and cofactor regeneration by Pt/Al_2O_3. Continuous processing has been highlighted as crucial for the sustainable manufacture of chemicals and is now a primary area for process development[33] because continuous operation overcomes the drawback of unproductive "down time" between batches, which is an imperative for the application of large scale biocatalysis in industry.[34] Without cofactor regeneration propanol production is limited by the initial NADH concentration (**Figure 7**). Propanol production with a continuous feed was achieved through the combined catalytic action of Pt/Al_2O_3 and alcohol dehydrogenase (**Figure 7a**) where a constant level of propanol production was maintained in operation for up to 100 h. The overall turnover number for NADH is 7, suggesting that further improvement would be beneficial. In another experiment, the reaction was started *without* NADH and the supply of cofactor was entirely dependent on regeneration from NAD^+ (**Figure 7b**). The formation of propanol has been increasing progressively while the control without Pt/Al_2O_3 showed no propanol produced. The results once again proved that the cofactor regeneration using heterogeneous catalysis was successful and the regenerated NADH was active.

As a proof of concept, this study demonstrates mutual compatibility and stability for the synthetic and enzymatic catalytic components. We can note recent work by Roche *et al.*[35] that examined NADH regeneration using immobilized FDH in a continuously supplied reactor for the enzymatic reduction of pyruvate to L-lactate. Starting with NAD^+ the immobilized FDH exhibited a much lower activity (2.0×10^{-5} - 5.5×10^{-5} μmol min^{-1}) than achieved in this

study with a significant loss (by 65%) of activity over 20 days. Liu *et al.*[36] have reported the coupling of photocatalytic regeneration (using carbon nitride prepared *via* fluoride etching) with enzymatic reduction of formaldehyde to methanol at a small (3 cm^3) scale. This system required $[Cp^*Rh(bpy)H_2O]^{2+}$, triethanolamine and a high photocatalyst loading (3 mg) with alcohol dehydrogenase (0.15 mg ml^{-1}) to achieve a rate of 0.21 μmol min^{-1} mg_{enzyme}^{-1}.

Our encouraging results from the fed-batch operation suggest that this combined enzymatic-heterogeneous catalytic system can be developed further for wide range of NADH-dependent enzymatic syntheses at a larger scale. This can potentially close the sustainability gap in cofactor utilization in enzymatic reduction processes. Further research has been set out to focus on the application of this coupled system to the production of chiral alcohols, exploiting the full potential of enzymatic catalysis.

4. Conclusions

This study has established for the first time the viability of heterogeneous catalytic (using Pt/Al_2O_3 and H_2) enzyme cofactor (NADH) regeneration. This procedure exhibits advantages in terms of full selectivity, stability, waste minimization (H^+ as sole by-product), facile catalyst separation and process sustainability (circumventing toxic metal complexes, electron mediators, sacrificial electron donors and photosensitizers). Cofactor regeneration using Pt/Al_2O_3 can be operated under ambient conditions and a wide range of pH (4–9.9) which facilitate coupling with enzymatic reaction. We have demonstrated the feasibility of incorporating *in situ* regeneration with an enzymatic process (reduction of propanal to propanol by alcohol dehydrogenase) in continuous (fed-batch) operation. Our methodology delivers effective NADH utilization with potential cost savings and paves new alternative pathways for cofactor regeneration.

Acknowledgements

The authors acknowledge financial support from the Scottish Carbon Capture and Storage (SCCS) program. Assistance from Dr. Sam Macfadzean, University of Glasgow, on STEM imaging of Pt/Al_2O_3 catalyst is also acknowledged.

References

(1) Bornscheuer, U. T.; Huisman, G. W.; Kazlauskas, R. J.; Lutz, S.; Moore, J. C.; Robins, K. *Nature* **2012**, *485*, 185-194.

(2) Gamenara, D.; Seoane, G. A.; Saenz-Méndez, P.; de María, P. D. In *Redox Biocatalysis*; John Wiley & Sons, Inc.: Hoboken, New Jersey, 2012, p 1-85.

(3) Faber, K. In *Biotransformations in Organic Chemistry*; Springer: Berlin/Heidelberg, 2011, p 31-313.

(4) (a) Hollmann, F.; Arends, I. W. C. E.; Holtmann, D. *Green Chem.* **2011**, *13*, 2285-2314. (b) De Wildeman, S. M.; Sonke, T.; Schoemaker, H. E.; May, O. *Acc. Chem. Res.* **2007**, *40*, 1260-1266.

(5) Wang, Y.; Li, L.; Ma, C.; Gao, C.; Tao, F.; Xu, P. *Sci. Rep.* **2013**, *3*, 2643.

(6) Moore, J. C.; Pollard, D. J.; Kosjek, B.; Devine, P. N. *Acc. Chem. Res.* **2007**, *40*, 1412-1419.

(7) Wu, H.; Tian, C.; Song, X.; Liu, C.; Yang, D.; Jiang, Z. *Green Chem.* **2013**, *15*, 1773-1789.

(8) (a) Lu, L.-Q.; Li, Y.; Junge, K.; Beller, M. *Angew. Chem. Int. Ed.* **2013**, *52*, 8382-8386. (b) Yan, Y.; Melchart, M.; Habtemariam, A.; Peacock, A. A.; Sadler, P. *J. Biol. Inorg. Chem.* **2006**, *11*, 483-488.

(9) (a) Oppelt, K. T.; Gasiorowski, J.; Egbe, D. A. M.; Kollender, J. P.; Himmelsbach, M.; Hassel, A. W.; Sariciftci, N. S.; Knör, G. *J. Am. Chem. Soc.* **2014**, *136*, 12721-12729. (b) Liu, J.; Antonietti, M. *Energy Environ. Sci.* **2013**, *6*, 1486-1493. (c) Huang, J.; Antonietti, M.; Liu, J. *J. Mater. Chem. A* **2014**, *2*, 7686-7693.

(10) (a) Ali, I.; Omanovic, S. *Int. J. Electrochem. Sci.* **2013**, *8*, 4283-4304. (b) Ali, I.; Khan, T.; Omanovic, S. *J. Mol. Catal. A: Chem.* **2014**, *387*, 86-91.

(11) (a) Steckhan, E.; Herrmann, S.; Ruppert, R.; Dietz, E.; Frede, M.; Spika, E. *Organometallics* **1991**, *10*, 1568-1577. (b) Wienkamp, R.; Steckhan, E. *Angew. Chem. Int. Ed.* **1982**, *21*, 782-783. (c) Hollmann, F.; Witholt, B.; Schmid, A. *J. Mol. Catal. B: Enzym.* **2002**, *19–20*, 167-176. (d) Hildebrand, F.; Lütz, S. *Chem-Eur. J.* **2009**, *15*, 4998-5001.

(12) (a) Lauterbach, L.; Lenz, O.; Vincent, K. A. *FEBS J.* **2013**, *280*, 3058-3068. (b) Hollmann, F.; Arends, I. W. C. E.; Buehler, K. *ChemCatChem* **2010**, *2*, 762-782.

(13) Irfan, M.; Petricci, E.; Glasnov, T. N.; Taddei, M.; Kappe, C. O. *Eur. J. Org. Chem.* **2009**, *2009*, 1327-1334.

(14) Reeve, H. A.; Lauterbach, L.; Lenz, O.; Vincent, K. A. *ChemCatChem* **2015**, *7*, 3480-3487.

(15) Bhoware, S. S.; Kim, K. Y.; Kim, J. A.; Wu, Q.; Kim, J. *J. Phys. Chem. C* **2011**, *115*, 2553-2557.

(16) Song, H.-K.; Lee, S. H.; Won, K.; Park, J. H.; Kim, J. K.; Lee, H.; Moon, S.-J.; Kim, D. K.; Park, C. B. *Angew. Chem. Int. Ed.* **2008**, *47*, 1749-1752.

(17) Maenaka, Y.; Suenobu, T.; Fukuzumi, S. *J. Am. Chem. Soc.* **2012**, *134*, 367-374.

(18) (a) Damian, A.; Maloo, K.; Omanovic, S. *Chem. Biochem. Eng. Q.* **2007**, *21*, 21-32. (b) Ali, I.; McArthur, M.; Hordy, N.; Coulombe, S.; Omanovic, S. *Int. J. Electrochem. Sci.* **2012**, *7*, 7675-7683.

(19) Gómez-Quero, S.; Cárdenas-Lizana, F.; Keane, M. A. *Ind. Eng. Chem. Res.* **2008**, *47*, 6841-6853.

(20) (a) Matam, S. K.; Kondratenko, E. V.; Aguirre, M. H.; Hug, P.; Rentsch, D.; Winkler, A.; Weidenkaff, A.; Ferri, D. *Appl. Catal. B: Environ.* **2013**, *129*, 214-224. (b) Hu, L.; Boateng, K. A.; Hill, J. M. *J. Mol. Catal. A: Chem.* **2006**, *259*, 51-60.

(21) Perret, N.; Cárdenas-Lizana, F.; Keane, M. A. *Catal. Commun.* **2011**, *16*, 159-164.

(22) Punyawudho, K.; Blom, D. A.; Van Zee, J. W.; Monnier, J. R. *Electrochim. Acta* **2010**, *55*, 5349-5356.

(23) (a) Soldevila-Barreda, J. J.; Romero-Canelón, I.; Habtemariam, A.; Sadler, P. J. *Nat. Commun.* **2015**, *6*, 6582. (b) de Graaf, R. A.; Behar, K. L. *NMR Biomed.* **2014**, *27*, 802-809.

(24) Bommarius, A. S.; Riebel, B. R. *Biocatalysis: Fundamentals and applications*; WILEY-VCH: Weinheim, 2004.

(25) Cheikhou, K.; Tzédakis, T. *AIChE J.* **2008**, *54*, 1365-1376.

(26) Soldevila-Barreda, J. J.; Bruijnincx, P. C. A.; Habtemariam, A.; Clarkson, G. J.; Deeth,

R. J.; Sadler, P. J. *Organometallics* **2012**, *31*, 5958-5967.

(27) Becker, E. D. *High Resolution NMR: Theory and Chemical Applications*; 3rd ed.; Elsevier Science: San Diego, 1999.

(28) Baranenko, V. I.; Kirov, V. S. *Atom. Energy* **1989**, *66*, 30-34.

(29) Reeve, H. A.; Lauterbach, L.; Ash, P. A.; Lenz, O.; Vincent, K. A. *Chem. Commun.* **2012**, *48*, 1589-1591.

(30) Maenaka, Y.; Suenobu, T.; Fukuzumi, S. *J. Am. Chem. Soc.* **2012**, *134*, 9417-9427.

(31) (a) Quinto, T.; Köhler, V.; Ward, T. *Top. Catal.* **2014**, *57*, 321-331. (b) Denard, C. A.; Hartwig, J. F.; Zhao, H. *ACS Catal.* **2013**, *3*, 2856-2864.

(32) de Torres, M.; Dimroth, J.; Arends, I. W. C. E.; Keilitz, J.; Hollmann, F. *Molecules* **2012**, *17*, 9835-9841.

(33) Newman, S. G.; Jensen, K. F. *Green Chem.* **2013**, *15*, 1456-1472.

(34) Homaei, A.; Sariri, R.; Vianello, F.; Stevanato, R. *J. Chem. Biol.* **2013**, *6*, 185-205.

(35) Roche, J.; Groenen-Serrano, K.; Reynes, O.; Chauvet, F.; Tzedakis, T. *Chem. Eng. J.* **2014**, *239*, 216-225.

(36) Liu, J.; Cazelles, R.; Chen, Z. P.; Zhou, H.; Galarneau, A.; Antonietti, M. *Phys. Chem. Chem. Phys.* **2014**, *16*, 14699-14705.

Table 1: Amount of reagent (in cm^3) required for the preparation of the lipoamide dehydrogenase assay.

Reagent	Blank	A_0	A	A'_0	A'
A (buffer)	2.0	1.0	0	1.0	0
B (DL-Thio)	0.2	0.2	0.2	0.2	0.2
C (EDTA)	0.1	0.1	0.1	0.1	0.1
D (product)	0	1.0	1.0	0	0
E (LDH)	0	0	1.0	0	1.0
F (positive control)	0	0	0	1.0	1.0

Table 2: Physicochemical characteristics of Pt/Al_2O_3.

	Pt/Al_2O_3 (as received)	Pt/Al_2O_3 (treated in H_2 at 350 °C)
Specific surface area ($m^2\ g^{-1}$)	162	175
Pore volume ($cm^3\ g^{-1}$)	0.40	0.43
Mean pore size (nm)	7.8	8.0
d (nm)	2.2	3.4
H_2 chemisorption ($\mu mol\ g^{-1}$)	4.1	21.5

Table 3: Rate and yield of propanol from propanal reduction with an enzyme/NADH/Pt/Al_2O_3 component matrix. Row **1**: control without enzyme; row **2**: enzymatic production of propanol without cofactor regeneration; row **3**: reaction with cofactor regeneration. *Reaction conditions*: T = 20 °C, pH = 8.8, P = 1 atm.

	Propanal (36 µL)	Enzyme (1 mg)	NADH (250 mg)	Pt/Al_2O_3 (25 mg)	Propanol production rate ($\mu mol_{propanol}\ min^{-1}\ mg_{enzyme}^{-1}$)	Propanol yield (%)
1	✓			✓	0.004[a]	0
2	✓	✓	✓		138	70
3	✓	✓	✓	✓	143	100

[a] units: $\mu mol_{propanol}\ min^{-1}\ mg_{Pt/Al_2O_3}^{-1}$

Figure 1

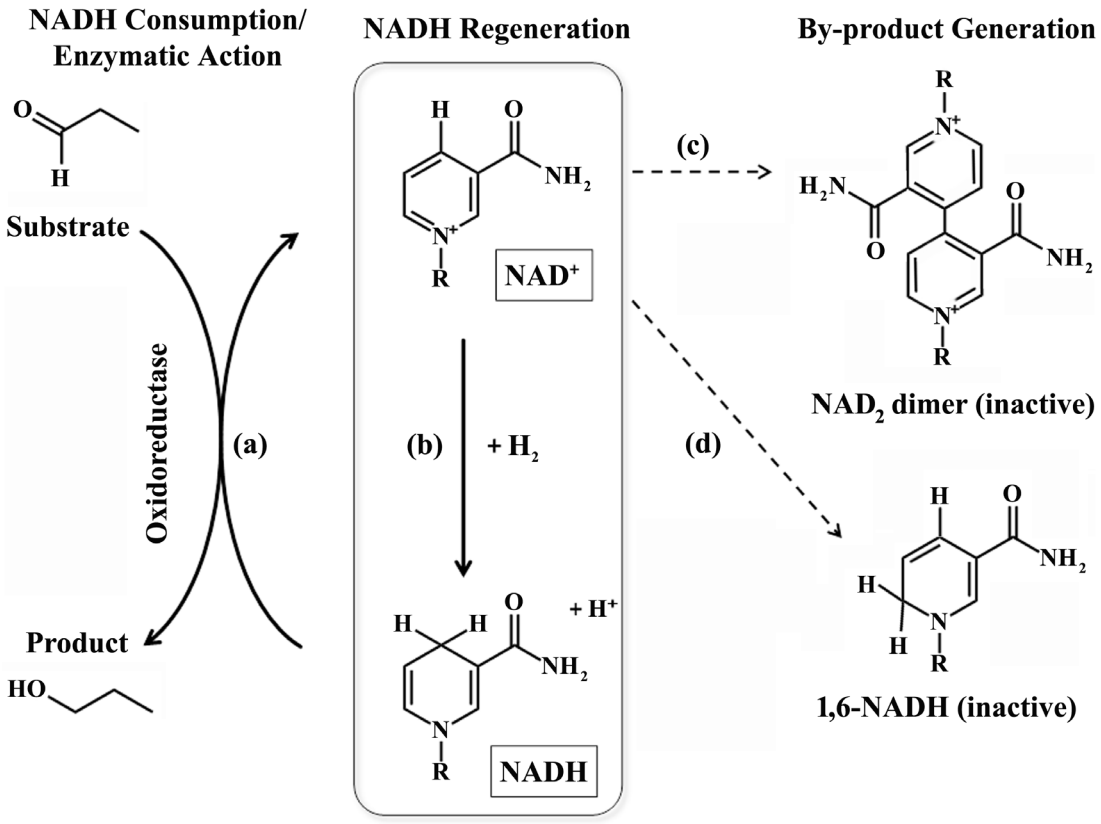

Figure 1: Schematic representation of (oxidoreductive) enzymatic reaction (propanal → propanol) using NADH as a cofactor and possible products obtained from NADH regeneration: **(a)** NADH consumption in oxidoreductase biotransformation; **(b)** target pathway for NADH regeneration; formation of undesired (dashed arrows) inactive **(c)** NAD_2 dimer and **(d)** 1,6-NADH. *Note*: R indicates adenosine diphosphoribose.

Figure 2

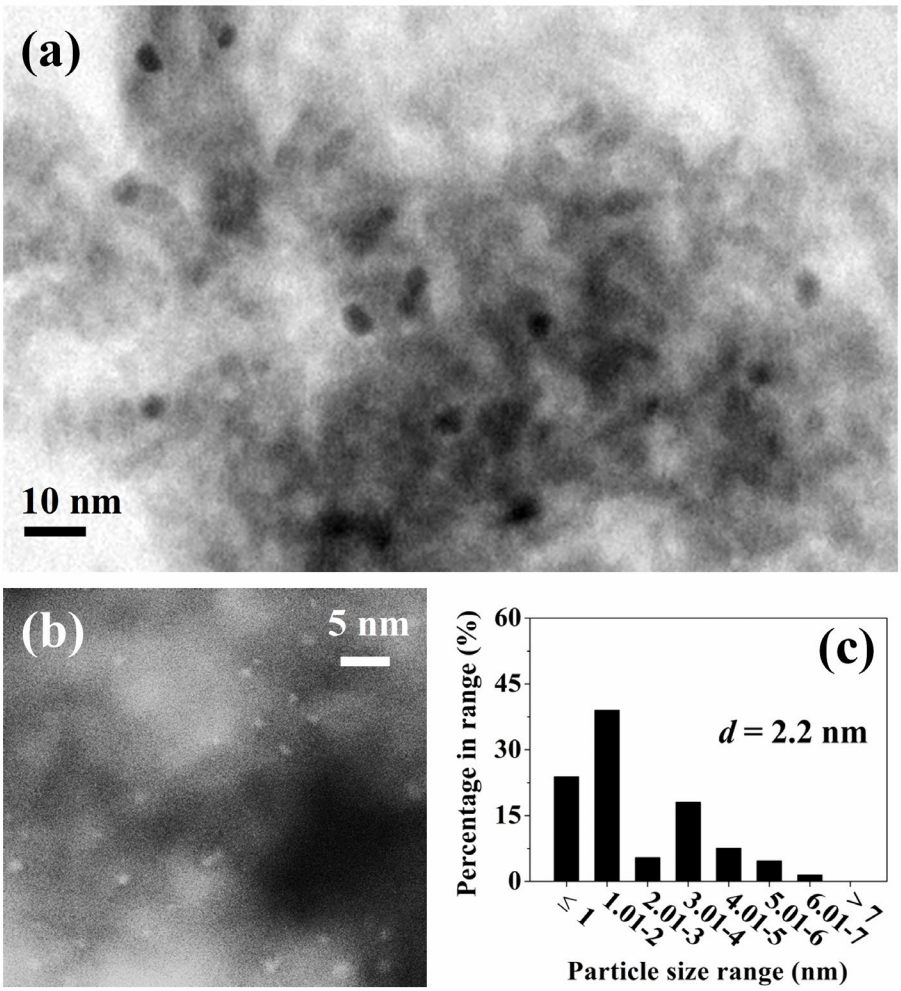

Figure 2: Representative STEM images of as received Pt/Al_2O_3 in bright field **(a)** and dark field **(b)** with associated Pt particle size distribution **(c)**.

Figure 3

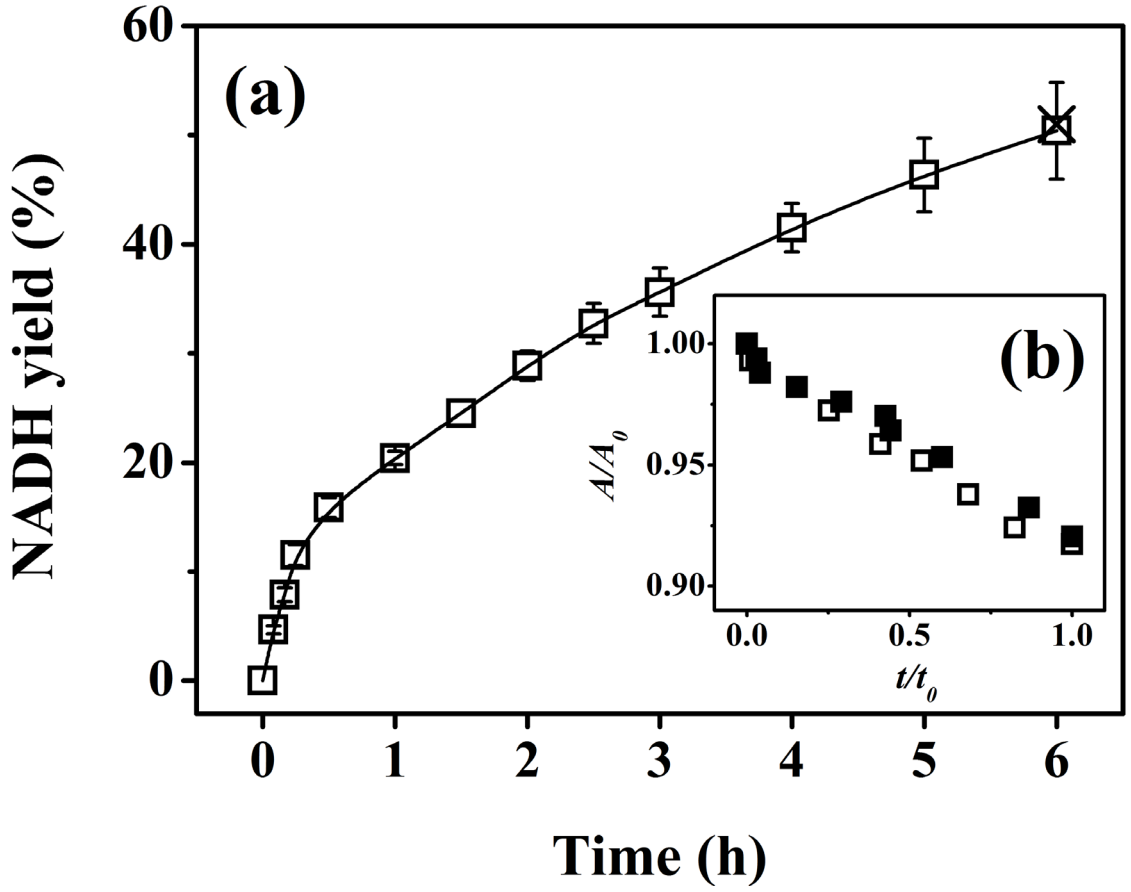

Figure 3: Pt/Al_2O_3 catalyzed $NAD^+ \rightarrow$ NADH regeneration. **(a)** Variation of NADH yield as a function of time (□, *Reaction conditions*: T = 37 °C, P = 9 atm, pH = 7, $[NAD^+]_0$ = 1.5 mM) with NADH yield determined by ^1H NMR (×); **(b)** NADH yield validation using enzymatic assay (EC 1.8.1.4): time dependence of normalized absorbance (A/A_0) of NADH produced experimentally (□) and from a prepared mixture using commercial NADH and NAD^+ (■, see Experimental Section): A_0 is the absorbance recorded before the enzymatic assay; A is the absorbance recorded after reaction is initiated; t_0 is the total run time of the enzymatic assay; t is the time after initiating the reaction (see Experimental Section).

Figure 4

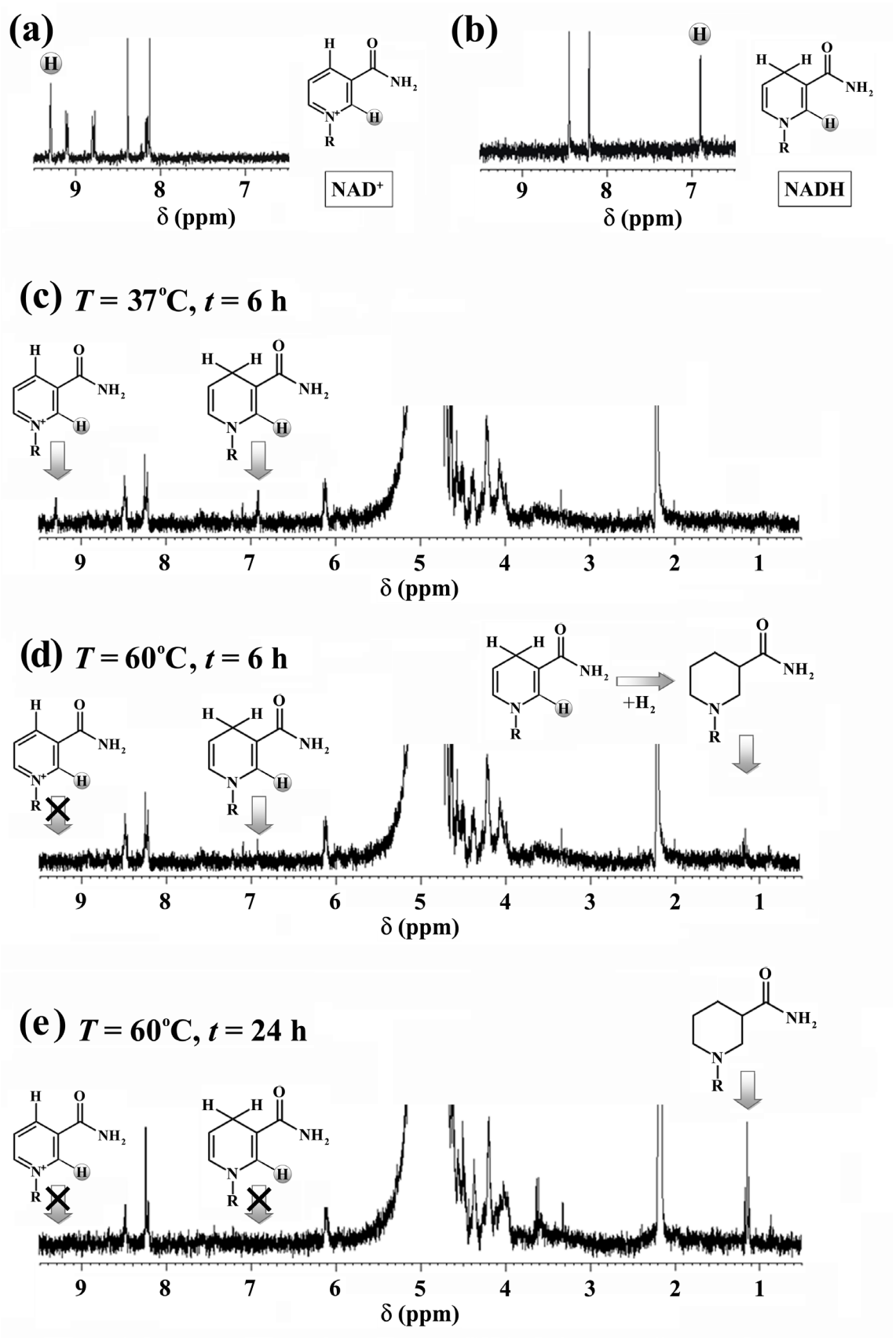
(a)
NAD+
δ (ppm)
(b)
NADH
δ (ppm)
(c) T = 37°C, t = 6 h
δ (ppm)
(d) T = 60°C, t = 6 h
+H2
δ (ppm)
(e) T = 60°C, t = 24 h
δ (ppm)

Figure 4: ^{1}H NMR spectra. **(a)** 1.5 mM NAD^{+} in 100 mM phosphate buffer (pH = 7.0); **(b)** 1.5 mM NADH in 100 mM phosphate buffer (pH = 7.0); reaction samples from Pt/Al_2O_3 promoted NAD^{+} reduction (P = 9 atm and pH = 7.0) at **(c)** 37 °C after 6 h and at 60 °C after **(d)** 6 h and **(e)** 24 h.

Figure 5

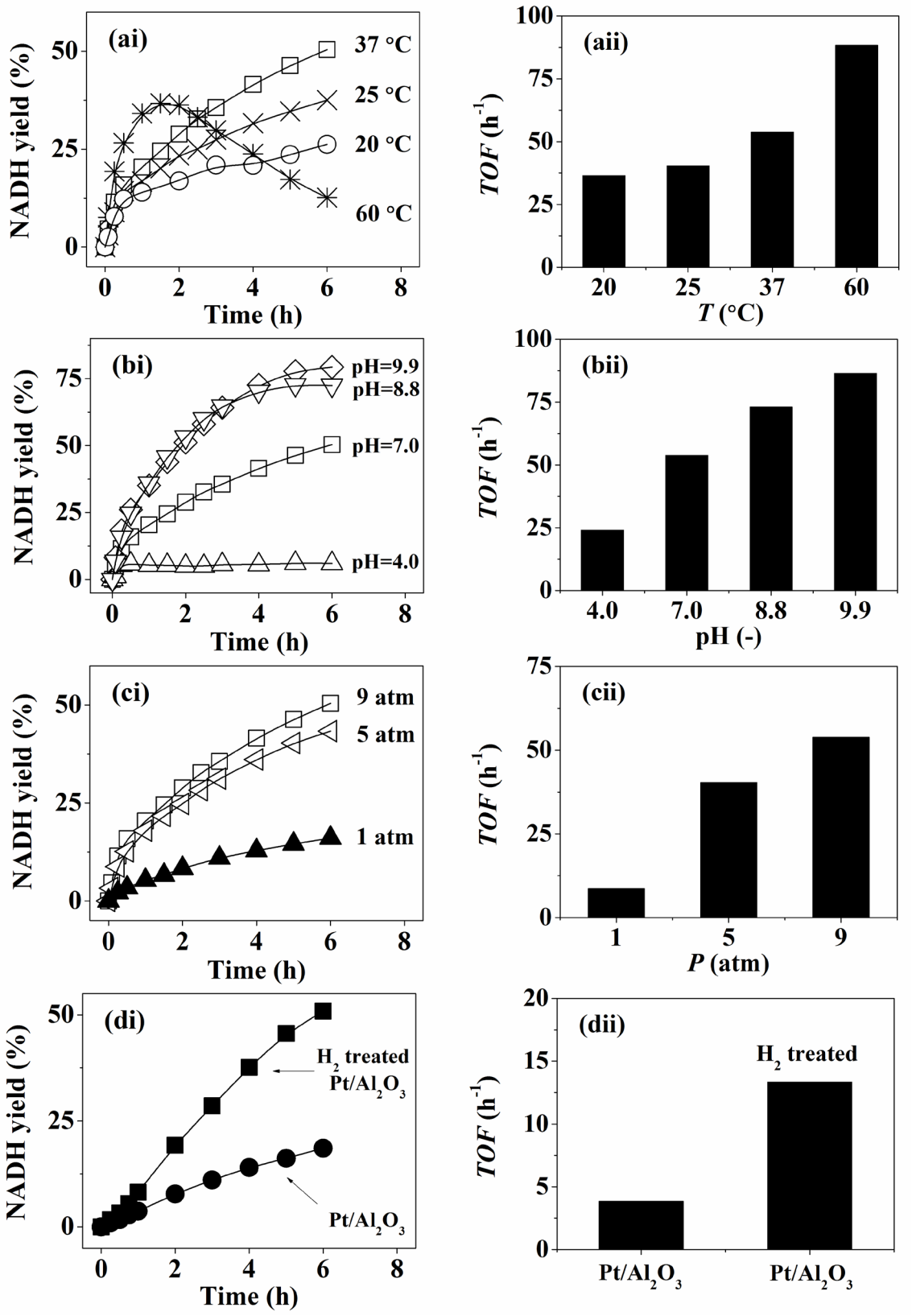

Figure 5: **(i)** Temporal variation of NADH yield and **(ii)** turnover frequency (*TOF*) as a function of: **(a)** temperature (20 °C (○) 25 °C (×), 37 °C (□) and 60 °C (✳) at *P* = 9 atm, pH = 7.0); **(b)** pH

(4.0 (△), 7.0 (□), 8.8 (▽) and 9.9 (◇) at T = 37 °C, P = 9 atm); **(c)** pressure, (1 atm (▲), 5 atm (◁) and 9 atm (□) at T = 37 °C, pH = 7.0); **(d)** H_2 treatment (Pt/Al_2O_3 as received (●) and H_2 treated Pt/Al_2O_3 (■) at T = 20 °C, P = 1 atm, pH = 8.8).

Figure 6

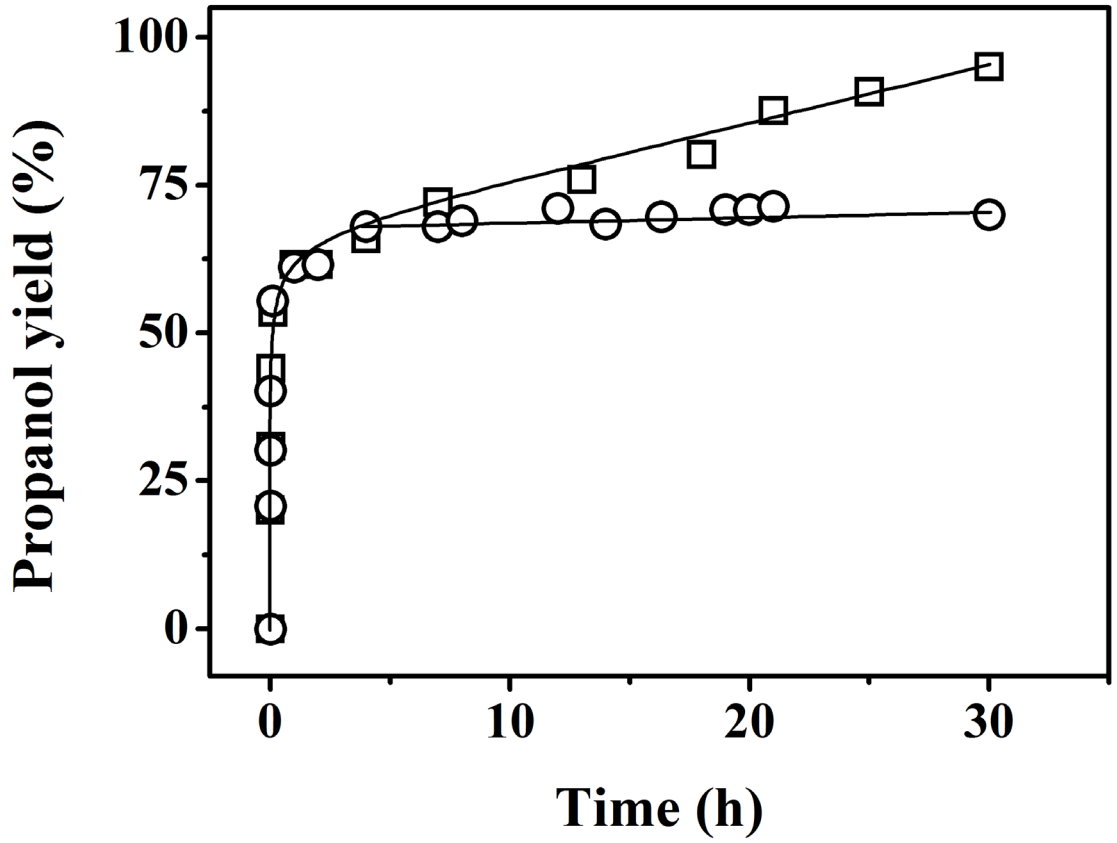

Figure 6: Batch enzymatic reduction of propanal to propanol coupled with *in situ* NADH regeneration by Pt/Al_2O_3. Temporal propanol yield over enzyme + NADH (○) and enzyme + NADH + H_2 + Pt/Al_2O_3 (□).

Figure 7

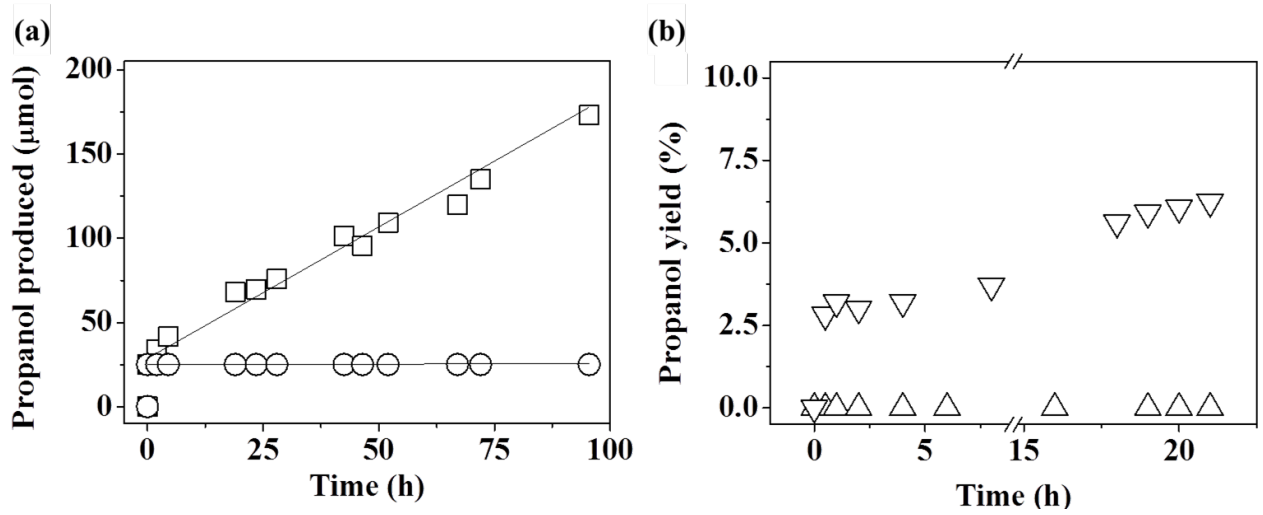

Figure 7: Continuous enzymatic reduction of propanal to propanol coupled with *in situ* NADH regeneration by Pt/Al_2O_3 in a fed-batch system. (a) Propanol production as a function of time with (□) and without (○) *in situ* NADH regeneration. (b) Temporal variation of propanol yield over alcohol dehydrogenase + NAD^+ (△) and alcohol dehydrogenase + NAD^+ + H_2 + Pt/Al_2O_3 (▽). Initial NAD^+: 330 mg. *Reaction conditions*: T = 20 °C, P = 1 atm, pH = 8.8 and propanal feed (concentration = 2 mM in buffer) rate = 2.5 cm^3 h^{-1}.

TOC figure:

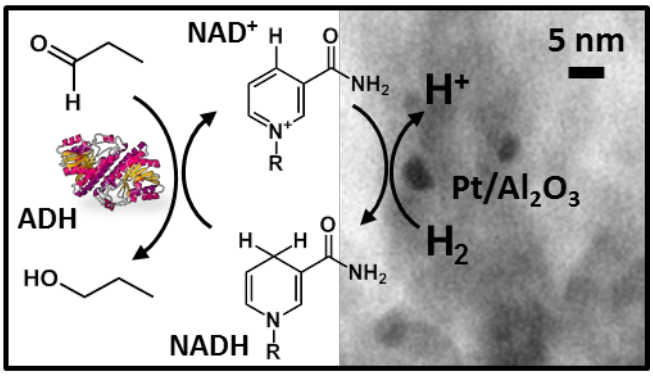

A hybrid inorganic-enzyme catalytic system was developed to reduce propanal to propanol with an *in situ* cofactor regeneration using Pt/Al_2O_3 as the catalyst.